Clinical Report

Journal of INTERNATIONAL MEDICAL RESEARCH

Journal of International Medical Research
2017, Vol. 45(4) 1347–1358

DOI: 10.1177/0300060517712654
journals.sagepub.com/home/imr
SAGE

Evaluation of cerebral glioma using 3T diffusion kurtosis tensor imaging and the relationship between diffusion kurtosis metrics and tumor cellularity

Chong Qi[1], Song Yang[1], Lanxi Meng[1], Huiyuan Chen[2], Zhenlan Li[1], Sijia Wang[1], Tao Jiang[1,3,4] and Shaowu Li[1,4]

Abstract

Purpose: To evaluate the clinical utility of diffusion kurtosis tensor imaging in the characterization of cerebral glioma and investigate correlations between diffusion and kurtosis metrics with tumor cellularity.

Materials and Methods: A group of 163 patients (age: 40.5 ± 11.5 years) diagnosed with cerebral glioma underwent diffusion kurtosis tensor imaging with a 3 T scanner. Diffusion and kurtosis metrics were measured in the solid part of tumors, and their abilities to distinguish between tumor grades was evaluated. In addition, we analyzed correlations between the metrics and tumor cellularity.

Results: Mean kurtosis (MK) revealed a significant difference between each pair of tumor grades ($P < 0.05$) and produced the best performance in a receiver operating characteristics analysis (area under the curve [AUC] = 0.89, sensitivity/specificity = 83.3/90). In contrast, mean diffusivity (MD) revealed a significant difference only for tumor grade II versus IV ($P < 0.05$). No significant differences between grades were detected with fractional anisotropy (FA; $P > 0.05$). Thus, kurtosis metrics exhibited a positive and strong correlation with tumor cellularity, while MD exhibited a negative or weak correlation with tumor cellularity.

Conclusion: Diffusion kurtosis metrics, particularly MK, demonstrated superior performance in distinguishing cerebral glioma of different grades compared with conventional diffusion metrics, and were closely associated with tumor cellularity.

[1]Beijing Neurosurgical Institute, Beijing Tiantan Hospital, Capital Medical University, Beijing, China
[2]Department of Neuropathology, Beijing Neurosurgical Institute, Beijing Tiantan Hospital, Capital Medical University, Beijing, China
[3]Department of Neurosurgery, Beijing Tiantan Hospital, Capital Medical University, Beijing, China
[4]National Clinical Research Center for Neurological Diseases, Beijing, China

Corresponding authors:
Shaowu Li and Tao Jiang, Tiantan Xili 6, Dongcheng District, Beijing, 100050, China; Beijing Neurosurgical Institute, Beijing Tiantan Hospital, Beijing, China.
Emails: lys_2016@sina.cn; taojiang1964@163.com

Keywords
Cerebral glioma, diffusion kurtosis imaging, magnetic resonance imaging, tumor cellularity

Date received: 28 January 2017; accepted: 9 May 2017

Introduction

Glioma is the most common type of brain tumor, comprising 30% of all brain and central nervous system (CNS) tumors, and 80% of all malignant brain tumors.[1] According to the World Health Organization (WHO) classification,[2] gliomas can be categorized into four grades (I–IV) based on histopathologic features, with high clinical significance for further treatment and prognosis. Gliomas are heterogeneous in nature, and histopathologic changes during malignant transformation of different grades contribute to the microstructural complexity of tumors.

Diffusion weighted (DW) and diffusion tensor (DT) magnetic resonance (MR) imaging have been utilized for the characterization and grading of gliomas,[3–9] assuming a Gaussian diffusion of water protons. However, in the examination of tissue complexity, cell membranes, organelles, and water compartments can act as barriers, causing compartmentalization and restricting the free displacement of water molecules, leading to a non-Gaussian diffusion of water.[10] Thus, conventional DT imaging (DTI) may have limitations for cases involving non-Gaussian diffusion due to complex tissue microstructure, and has been reported to lack sensitivity and specificity for monitoring cellular changes related to malignant progression.[4]

Diffusion kurtosis tensor imaging (DKT), as an extension of DTI, allows for the estimation of additional diffusion kurtosis metrics that can characterize non-Gaussian water diffusion behavior.[10] DKT has been found to exhibit successful performance in situations with a higher degree of tissue complexity in white matter compared with gray matter, with higher mean kurtosis (MK) values in white matter.[10] Changes of kurtosis metrics are believed to be strongly associated with tissue microstructure,[10–12] and DKT has been proposed as a method for examining glioma.[13–15] However, previous studies using DKT have been limited by relatively small patient sample sizes, and have not examined the relationships between diffusion metrics, kurtosis metrics, and tumor cellularity.[13–15]

The current study sought to characterize gliomas using DKT, investigating the relationships between available metrics and tumor cellularity with a large patient population.

Materials and methods

Patients

This study was approved by our institutional review board and written informed consent was obtained from all patients. Patients who were diagnosed with cerebral glioma at our outpatient clinic and treated in our hospital between January 2015 and March 2016 were considered for inclusion in the study. Patients with recurrent tumor or surgery prior to the MR examination were excluded. A total of 163 patients (101 men and 62 women, age: 40.5 ± 11.5 years; range, 13–72 years) who were scheduled to have surgery within 3 weeks were included in the study. Tissue samples were examined histopathologically by an experienced neuropathologist. Tumor grading was performed based on the WHO classification.[2]

MR Imaging

All patients underwent MR imaging using a 3.0 Tesla MR system (MAGNETOM PRISMA, Siemens Healthcare, Erlangen, Germany) with a commercial 64-channel

head/neck coil. MR protocols included: 1) fast low-angle shot (FLASH) sequence based T1-weighted imaging, field of view (FOV), $240 \times 240\,mm^2$; repetition time (TR)/echo time (TE), 8/3 ms; flip angle (FA), 70°; slice thickness, 1 mm; matrix size, 256 ×256; 2) Turbo spin echo (TSE) sequence based T2-weighted imaging, FOV, $256 \times 192\,mm^2$; TR/TE, 3500/102 ms; FA, 90°; slice thickness, 3 mm; matrix size, 448 × 358; 3) Fluid-attenuated inversion recovery (FLAIR), FOV, $256 \times 192\,mm^2$; TR/TE, 7000/79 ms; inversion time (TI), 2500 ms; FA, 120°; slice thickness, 4 mm with 0.4 mm gap; matrix size, 256 × 192; and 5) DKT was based on conventional DTI using a two-dimensional double spin-echo echo planar imaging (EPI) sequence to minimize the eddy current effect;[16] FOV, $220 \times 220\,mm^2$; TR/TE, 3600/76 ms; FA, 90°; number of slices, 25; slice thickness, 3 mm; slice distance factor: 30%; matrix size, 128 × 128; diffusion gradient encoding in 32 uniformly distributed directions with three b-values $(0, 1000, 2000\,s/mm^2)$ in each direction, average = 1 for each b-value; the total acquisition time was 13 minutes 6 seconds. The T1-weighted sequences were performed before and after the administration of 0.2 mmol per kilogram of body weight of gadopentetate dimeglumine (Magnevist; Berlex Laboratories, Wayne, NJ).

Imaging processing and analysis

First, motion correction and spatial smoothing (Gaussian filter with full width at half maximum of 2.5 mm) was performed for the DKT data using software (Statistical Parametric Mapping, University College London, London, England).[17] Conventional diffusion and kurtosis metrics were derived per voxel simultaneously using a constrained maximum likelihood algorithm,[18,19] resulting in parametric maps of mean diffusivity (MD; the apparent diffusion coefficient averaged over all directions), fractional anisotropy (FA), mean kurtosis (MK; the apparent kurtosis coefficient averaged over all directions), kurtosis along the axial direction (Kax) and kurtosis along the radial direction (Krad). All tensor metrics estimation was processed automatically using a custom Matlab (MathWorks, Natick, MA) program developed in-house.

A neurologist with 10 years of experience in MR imaging (MRI) interpretation delineated the solid part of the tumor exhibiting low T2 signal intensity, and the corresponding part of the contralateral normal-appearing white matter (NAWM) as regions of interest (ROIs) on T2-weighted images using SPIN (Signal Processing In NMR, Detroit, Michigan, USA) software. Care was taken to avoid edema and necrosis, which also exhibit hyperintensity on T2-weighted images. ROIs defined on T2-weighted images were then transferred to all parametric maps using affine registration[14] (Figure 1). Furthermore, all parameters in tumor ROIs were normalized for each patient (i.e., normalized parameters = average parameters [tumor]/average parameters [NAWM]), to mitigate the potential impact of inter-individual brain differences.

All ROI-related measurements were performed twice, with an interval of 3 days for the assessment of inter-observer agreement.

Histopathology and tumor cellularity

A single neuropathologist with 10 years of experience in neuropathology who was unaware of the previous MRI findings reviewed all the representative histological sections (200×) using an optical microscope (Nikon Eclipse E600, Nikon, Osaka, Japan). For each case, grades (II–IV) were assigned based on the representative histological sections according to the WHO classification.[2]

Tumor cellularity analysis was performed by an uninformed expert histologist (5 years of experience in histology) using Image Pro Plus (Version, 6.0, Media Cybernetics, Inc.,

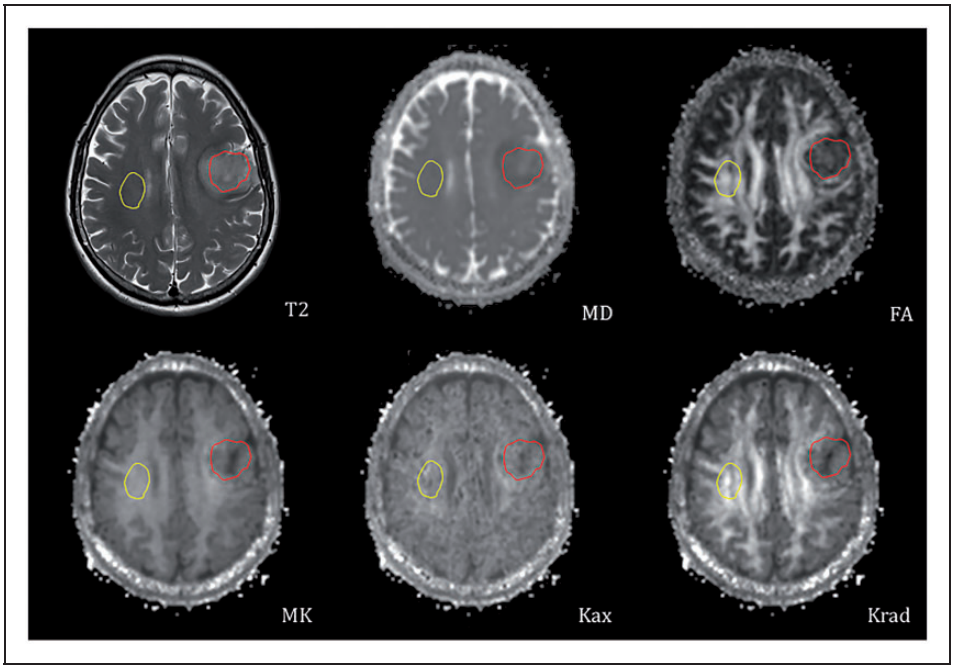

Figure 1. T2-weighted image and corresponding diffusion kurtosis parametric maps (MD, FA, MK, Kax and Krad) for a 60-year-old male with WHO-III glioma. Regions of interest (ROIs) were drawn in the solid part of the tumor (red) and contralateral normal appearing whiter matter (yellow), respectively.

MD, USA) software. Tumor cellularity was defined as the ratio of total area of the tumor cell nuclei to that of the histologic section. An adaptive histogram equalization and color intensity threshold was used to segment darker stained cell nuclei and automatically obtain the total area of the tumor cell nuclei and that of the histologic section (Figure 2).

Statistical analysis

All parameters in NAWM were corrected for age-related changes.[17] Tumor cellularity and the diffusion and kurtosis metrics, including MD, FA, MK, Kax, Krad and corresponding normalized values were compared among tumor grades using Mann-Whitney tests. Receiver operating characteristic (ROC) curves were used for the diffusion and kurtosis metrics and corresponding normalized values, and the area under the ROC curve (AUC) was calculated for the assessment of the optimal discriminating parameter for grade II versus III, grade III versus IV, and grade II versus IV tumors. The correlations between tumor cellularity and the diffusion and kurtosis metrics of the individual lesions were tested using a simple linear regression analysis. Intra-observer agreement in ROI-related measures was evaluated using the intraclass correlation coefficient (ICC) based on the measurement results at two different times. $P < 0.05$ was considered to indicate significant difference. All statistical analyses were performed using MedCalc Statistical Software version 15.6.1 (MedCalc Software bvba, Ostend, Belgium; https://www.medcalc.org; 2015).

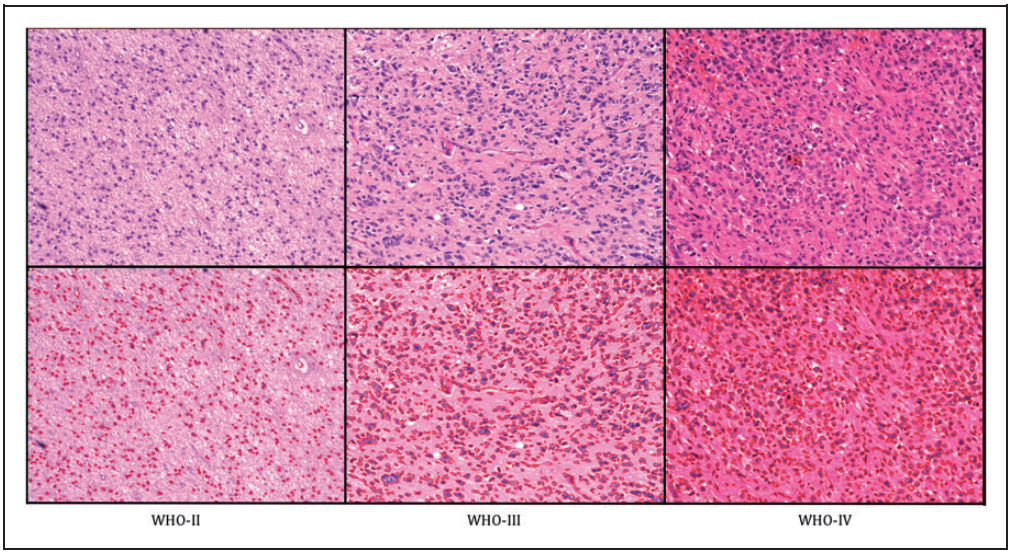

Figure 2. Histological slides (200×) stained with hematoxylin and eosin (H&E) for three typical cases: a 42-year-old woman with WHO-II glioma (top left), a 48-year-old man with WHO-III glioma (top middle) and a 63-year-old man with WHO-IV glioma (top right). Tumor cell nuclei in these three cases were automatically segmented (red boundaries) using software (WHO-II glioma, bottom left; WHO-III glioma, bottom middle; WHO-IV glioma, bottom right).

Results

The pathological examinations revealed that 63 of 163 patients (38.7%) met the criteria for WHO II glioma (astrocytoma), 48 patients (29.4 %) met the criteria for WHO III gliomas (astrocytoma), and 52 patients (31.9 %) met the criteria for WHO IV (glioblastoma multiforme, GBM).

Contrast enhancement was observed in 141 gliomas (grade II: 41, grade III: 48 and grade IV: 52, 87% of all patients), whereas 22 gliomas (grade II: 22, 13% of all patients) were not found to be enhanced during the MR examination but were confirmed by histological examination. A case of WHO III glioma with a contrast-enhanced T1-weighted image and corresponding diffusion kurtosis parametric (MD, FA, MK, Kax and Krad) maps is shown in (Figure 3).

The age of patients differed significantly between the three groups (grade II, 33.2 years; grade III, 43.1 years; grade IV, 46.9 years, $P < 0.01$), and all NAWM metrics were found to correlate with age (MD: $r = 0.39$, $P = 0.003$; FA: $r = -0.22$, $P = 0.04$; MK: $r = -0.18$, $P = 0.02$; Kax: $r = -0.20$, $P = 0.02$; Krad: $r = -0.28$, $P = 0.04$). Therefore, age-correction for all metrics in NAWM was performed with the average age of all patients (40.5 years) and the slope of the linear regression of the metrics versus age.

The average and normalized metrics and tumor cellularity in each grade group are summarized in Table 1. Tumor cellularity increased with grade, with mean values of $11.6\% \pm 4.8\%$, $20.8\% \pm 7.2\%$ and $29.9\% \pm 7.7\%$, for grade II, III, and IV, respectively. Distributions of diffusion and kurtosis metrics in NAWM and tumors with different grades are shown in Figure 4. Table 2 shows a summary of the comparison between diffusion and kurtosis metrics and tumor cellularity among different tumor grades. Tumor cellularity differed significantly in each grade ($P < 0.001$). No significant

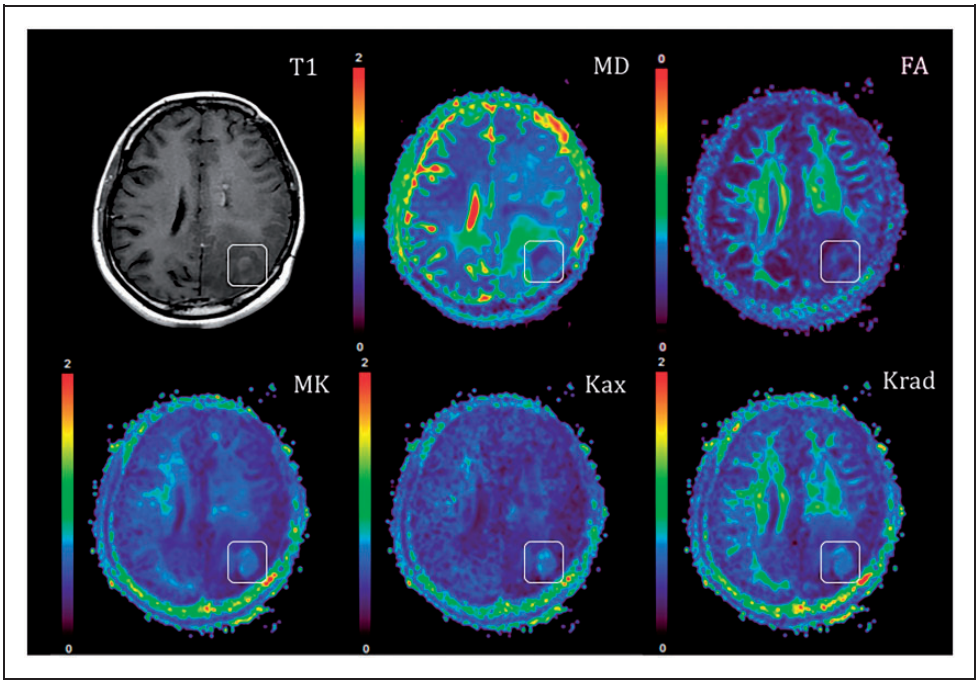

Figure 3. Post-contrast T1-weighted image and corresponding diffusion kurtosis parametric maps for a 36-year-old woman with WHO III glioma. The solid part of the tumor (white square) was slightly enhanced on T1-weighted image and showed different contrast on MD, FA and kurtosis parametric maps. The MD bar is shown in units of 10^{-3} mm^2/s, while the bars of other maps have dimensionless units.

Table 1. Diffusion kurtosis metrics in different tissue types and corresponding tumor cellularity.

	MD (10^{-3} mm^2/s)	FA	MK	Kax	Krad	Tumor Cellularity (%)
NAWM	0.91 ± 0.06	0.40 ± 0.10	1.00 ± 0.11	0.77 ± 0.90	1.32 ± 0.24	N.A.
WHO II	1.62 ± 0.44	0.12 ± 0.09	0.52 ± 0.18	0.51 ± 0.15	0.55 ± 0.24	11.6 ± 4.8
	(1.80 ± 0.50)	(0.30 ± 0.23)	(0.53 ± 0.20)	(0.68 ± 0.23)	(0.43 ± 0.20)	
WHO III	1.45 ± 0.43	0.13 ± 0.04	0.62 ± 0.21	0.59 ± 0.17	0.64 ± 0.23	20.8 ± 7.2
	(1.58 ± 0.47)	(0.33 ± 0.1)	(0.63 ± 0.20)	(0.79 ± 0.28)	(0.49 ± 0.16)	
WHO IV	1.34 ± 0.28	0.12 ± 0.03	0.72 ± 0.18	0.70 ± 0.18	0.73 ± 0.19	29.9 ± 7.7
	(1.48 ± 0.35)	(0.30 ± 0.12)	(0.71 ± 0.23)	(0.93 ± 0.31)	(0.58 ± 0.22)	

Note: Values are presented as mean ± standard deviation; NAWM – normal appearing white matter; MD/MK – mean diffusion and kurtosis parameters derived from DKI images; Krad – radial kurtosis, Kax – axial kurtosis, and tumor cellularity – the nuclei-to-cytoplasm ratio. The normalized values are presented in parentheses.

difference was found for FA/normalized FA between each pair of grades ($P > 0.05$). For grade II versus III, only MK/normalized MK was found to exhibit a significant difference ($P = 0.03/0.04$); other parameters, including MD/normalized MD, Kax/normalized Kax, and Krad/normalized krad, did not exhibit significant differences

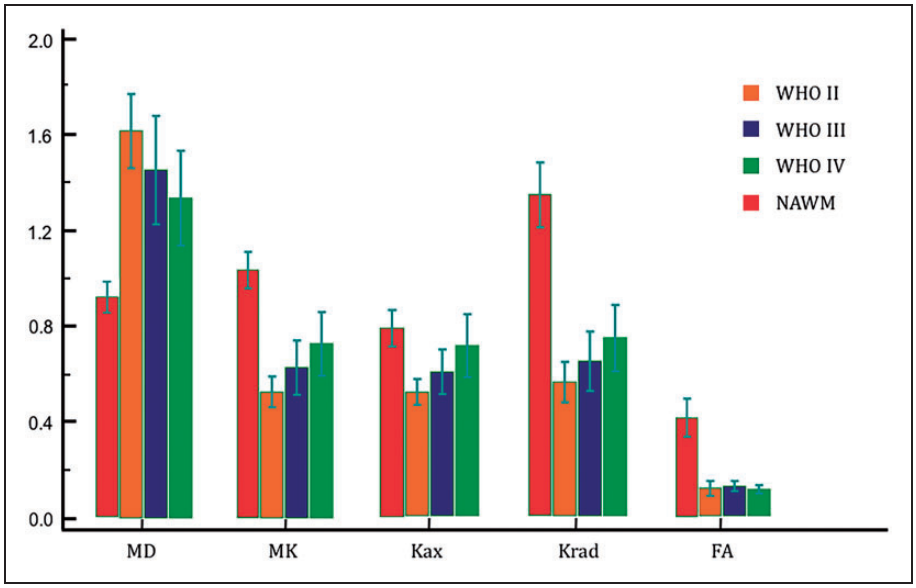

Figure 4. Box-and-whisker plot distribution for the diffusion and kurtosis metrics in normal appearing white matter (NAWM) and tumors with different grades.

Table 2. Sample tests of differences in diffusion kurtosis metrics and cellularity in tumors of different grades.

Parameters	II versus III (*P* value)	II versus IV (*P* value)	III versus IV (*P* value)
MD	0.26 (0.22)	0.04 (0.03)	0.34 (0.53)
FA	0.06 (0.13)	0.24 (0.36)	0.54 (0.53)
MK	0.03 (0.04)	0.006 (0.02)	0.02 (0.04)
Kax	0.07 (0.1)	0.006 (0.02)	0.01 (0.03)
Krad	0.1 (0.16)	0.02 (0.04)	0.02 (0.03)
Tumor cellularity	<0.001	<0.001	<0.001

Note: MD and MK – mean diffusion and kurtosis coefficients; FA – Fractional anisotropy; Kax – kurtosis in the axial direction; Krad – kurtosis in the radial direction; tumor cellularity is defined as the ratio of the area of tumor cell nuclei to the area of cytoplasm. *P*-values for the results of normalized parameters are presented in parentheses.

($P > 0.05$). For grade II versus IV, most parameters, including MD/normalized MD, MK/normalized MK, Kax/normalized Kax and Krad/normalized Krad, exhibited significant differences ($P < 0.05$). For grade III versus IV, MK/normalized MK ($P = 0.02/0.04$), Kax/normalized Kax ($P = 0.01/0.03$) and Krad/normalized Krad ($P = 0.02/0.03$) exhibited significant differences.

ROC curves of the diffusion kurtosis metrics for distinguishing between tumors of different grades are shown in Figure 5, with detailed information presented in Table 3.

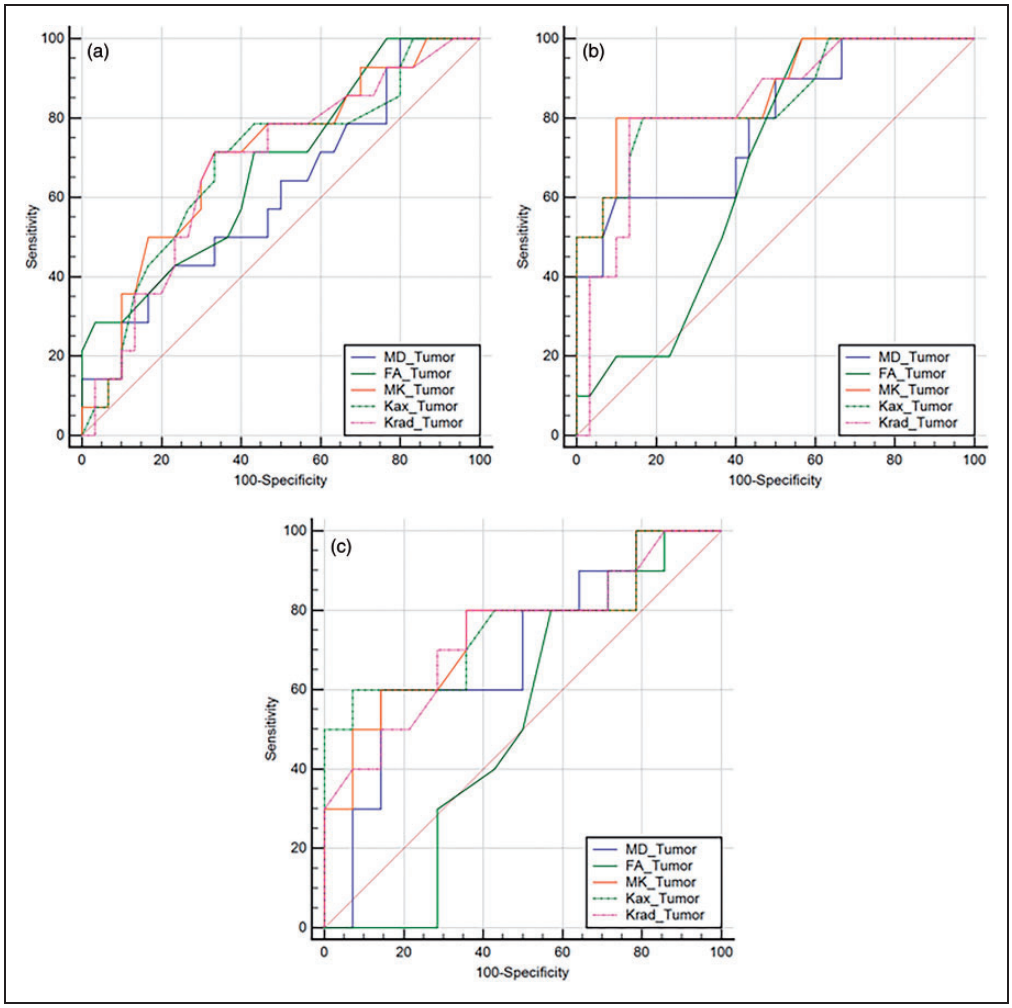

Figure 5. Receive operating characteristic curves for the diffusion and kurtosis metrics in differentiating between a) Grade II versus III; b) Grade II versus IV and c) Grade III versus IV. The curve for MK demonstrated the best performance for differentiating between each pair of grades.

The analysis of correlations between all metrics and tumor cellularity revealed that MK/normalized MK ($r = 0.47/0.46$, $P = 0.003/0.003$) and Kax/normalized Kax ($r = 0.45/0.48$, $P = 0.004/0.002$) exhibited stronger correlations than Krad/normalized Krad ($r = 0.37/0.37$, $P = 0.02/0.02$) and MD/normalized MD ($r = -0.33/0.34$, $P = 0.04/0.03$), while FA/normalized FA ($r = 0.36/0.30$, $P = 0.02/0.06$) exhibited a weak correlation.

The analysis of ROI-related measures revealed that the mean intraclass correlation coefficient was 0.851 (range, 0.832–0.902), suggesting good intraobserver agreement. Therefore, all results were based on the average of two readers' observations.

Discussion

The current results demonstrated that kurtosis metrics (MK/normalized MK, Kax/

Table 3. Receiver operating characteristic (ROC) curve analysis of differences in diffusion and kurtosis metrics between different tumor grades (II vs. III, II vs. IV and III vs. IV).

Parameters		AUC*	Threshold	Sensitivity (%)	Specificity (%)	*P* value
MD	II vs. III	0.599/0.608	1.37/1.82(10^{-3}mm^2/s)	50/75	67.65/47.06	0.26/0.21
	II vs. IV	0.703/0.712	1.28/1.43(10^{-3}mm^2/s)	60/70	79.41/73.53	0.03/0.02
	III vs. IV	0.613/0.575	1.28/1.43(10^{-3}mm^2/s)	60/70	75/68.75	0.33/0.53
FA	II vs. III	0.665/0.691	0.09/0.3	75/62.5	52.94/76.47	0.04/0.01
	II vs. IV	0.624/0.597	0.08/0.22	100/70	41.18/52.94	0.14/0.33
	III vs. IV	0.572/0.575	0.12/0.27	80/60	50/62.5	0.53/0.55
MK	II vs. III	0.74/0.78	0.5/0.46	75/87.5	66.67/60	0.003/0.02
	II vs. IV	0.89/0.85	0.6/0.52	83.3/80	90/84.71	0.0001/0.004
	III vs. IV	0.72/0.70	0.67/0.75	66.7/60	75/88.8	0.04/0.03
Kax	II vs. III	0.66/0.644	0.48/0.56	73.3/87.5	60.6/41.18	0.06/0.09
	II vs. IV	0.84/0.76	0.55/0.95	83.3/60	75.8/91.18	0.0001/0.02
	III vs. IV	0.72/0.64	0.68/0.95	66.7/60	81.2/81.25	0.04/0.02
Krad	II vs. III	0.64/0.624	0.52/0.34	73.3/81.25	60.6/50	0.11/0.12
	II vs. IV	0.79/0.74	0.6/0.44	83.3/80	78.8/61.76	0.0001/0.02
	III vs. IV	0.72/0.70	0.58/0.48	83.3/73.5	56.2/62.5	0.03/0.03

*Area under ROC curves; MD and MK – mean diffusion and kurtosis coefficients; FA – Fractional anisotropy; Kax – kurtosis in the axial direction; Krad – kurtosis in the radial direction; For each parameter, three rows of values correspond to II versus III, II versus IV and III versus IV respectively.

normalized Kax and Krad/normalized Krad) increased with tumor grade. Only MK/normalized MK significantly differed between each pair of tumor grades ($P < 0.05$) and demonstrated the best performance in discrimination of tumor grades with respect to the ROC curve analysis. In addition, in contrast to MK/normalized MK, neither Kax/normalized Kax or Krad/normalized Krad detected significant differences between tumor grades II and III, and produced ROC results with less statistical power. As a possible explanation, because Kax and Krad are designed to specifically address direction-dependent tissue complexity, they may have less generalizability for tumor cases, compared with MK. In addition, the results revealed that MD/normalized MD decreased with tumor grade, and showed significant differences only between tumor grade II and IV ($P < 0.05$), with relatively weak ROC results compared with those of the kurtosis metrics. In a previous study, Raab et al.[13] found that MD only detected significant differences between tumor grades III and IV, while Van Cauter et al.[14] reported that MD was not significantly different between lower grade (II) and higher grade (III and IV) tumors. These discrepancies between previous studies of MD may have been caused by differences in sample size, differences in DKT protocols, or other factors affecting MD.[13,14,20–23] Regarding FA, variation has been reported between studies,[5,13,14] and the clinical utility of FA in glioma grading is contentious. In the current study, FA did not reveal significant differences between tumor groups, except between tumor grades II and III. FA is known to change with age and brain region.[5] These differences may act as a confounding factor in the evaluation of FA in glioma diagnosis, and may be responsible for variation between studies. The current finding that kurtosis metrics and FA were much higher in NAWM than in tumor ROIs, while MD in NAWM was much lower than in tumor ROIs, is in accord with

previous studies,[13–15,20] indicating that the degree of tissue complexity is decreased in tumor tissue compared with NAWM.

Since histologic examination is considered the standard protocol for glioma diagnosis and grading, the diagnosis of glioma using diffusion and kurtosis metrics was also evaluated in terms of tumor cellularity in the current study. The increase of tumor cellularity with tumor grade and the significant differences between every pair of grades may indicate an increase in cell membranes and organelles, or changes of intra- or extra cellular space with tumor grade,[24] all of which would be expected to affect water diffusion and contribute to the degree of tissue complexity.[11,12] MD values in tumors are likely to be affected by several factors. For instance, variations in molecular crowding and viscosity among different intercellular organelles have been found to affect MD at the intracellular level.[21] Moreover, changes in glandular fluid are thought to reduce MD in prostate cancer.[22] In a unique case, low MD was found to coexist with a small number of cells in pediatric brain tumor.[23] As such, MD may not be an appropriate measure for characterizing tumor cellularity or tumor grading. In the current study, kurtosis metrics including MK, Kax and Krad were negatively correlated with tumor cellularity, whereas MD and FA exhibited positive correlations with relatively weak statistical power. The stronger correlations between kurtosis parameters and tumor cellularity might be responsible for their superior performance in discriminating between tumor grades, and their higher diagnosis accuracy, in accord with the notion that tumor cellularity should be considered one of the features for determining histologic grade.[2]

Increased tumor cellularity would be expected to have a substantial impact on MD and kurtosis metrics because of restricted diffusion and high microstructural complexity. Therefore, MD and kurtosis metrics may be appropriate indicators, reflecting different aspects of diffusion.[10] Interestingly, Figure 3 shows a case of WHO III glioma with parametric maps providing different contrasts for the solid part of the tumor. On post-contrast T1-weighted images, the high concentration of contrast agent in the upper left part of the tumor resulted in an uneven contrast, indicating tumor heterogeneity. The MD map showed weak diffusion in the upper left part and relatively strong diffusion in the lower right part of the tumor. Similarly, the FA map showed less anisotropy in the lower right part of the tumor. However, corresponding kurtosis parametric maps showed relatively uniform contrast for the solid part of the tumor, reflecting a similar degree of microstructural complexity within. This comparison of contrast indirectly suggests that MD may be affected by factors other than tissue structure. However, no previous findings indicate that changes in MD are proportional to the degree of microstructural complexity, even without considering the other factors that may affect MD. Because diffusion kurtosis is not based on a specific model,[10] and it is difficult to establish a relationship between diffusion and the general concept of tissue complexity, the nature of diffusion kurtosis and its intrinsic association with diffusion requires further investigation. Although, the mechanisms underlying differences in MK changes within gliomas remain to be clarified, MK still can serve as a promising indicator of tumor grade.

Several limitations of the current study should be considered. First, although a large patient population was examined in this study, a multi-center study would be helpful for controlling for the potential confounding differences between single center studies. Second, it should be noted that the impact of tumor position on kurtosis metrics was not investigated in this study, possibly resulting in

position-dependent bias. Finally, as histopathological results are strongly affected by the specimen fixation protocol used, grade migration may have resulted from suboptimal fixation, which may adversely affect tumor grading.

In conclusion, the current results indicate that the kurtosis parameter MK is a useful index for tissue complexity, as a method for quantifying non-Gaussian diffusion behavior. We found that MK was the best-performing diffusion kurtosis parameter for characterizing cerebral glioma. However, the nature of non-Gaussian diffusion behavior and its intrinsic association with conventional diffusion requires further elucidation.

Acknowledgements

This project was supported by the National High Technology Research and Development Program of China (863 program) (2015AA020504).

Declaration of conflicting interests

The authors declare that there is no conflict of interest.

Funding

This project was supported by the National High Technology Research and Development Program of China (863 program) (2015AA020504) to Shaowu Li and Innovation Fund Project of Beijing Neurosurgical Institute (Institute Youth-2014017) to Chong Qi.

References

1. Goodenberger ML and Jenkins RB. Genetics of adult glioma. *Cancer Genet* 2012; 205: 613–621.
2. Louis DN, Ohgaki H, Wiestler OD, et al. The 2007 WHO classification of tumours of the central nervous system. *Acta Neuropathol* 2007; 114: 97–109.
3. Sadeghi N, D'Haene N, Decaestecker C, et al. Apparent diffusion coefficient and cerebral blood volume in brain gliomas: relation to tumor cell density and tumor microvessel density based on stereotactic biopsies. *AJNR Am J Neuroradiol* 2008; 29: 476–482.
4. Goebell E, Paustenbach S, Vaeterlein O, et al. Low-grade and anaplastic gliomas: differences in architecture evaluated with diffusion-tensor MR imaging. *Radiology* 2006; 239: 217–222.
5. Beppu T, Inoue T, Shibata Y, et al. Measurement of fractional anisotropy using diffusion tensor MRI in supratentorial astrocytic tumors. *J Neurooncol* 2003; 63: 109–116.
6. Sugahara T, Korogi Y, Kochi M, et al. Usefulness of diffusion-weighted MRI with echo-planar technique in the evaluation of cellularity in gliomas. *J Magn Reson Imaging* 1999; 9: 53–60.
7. Sinha S, Bastin ME, Whittle IR, et al. Diffusion tensor MR imaging of high-grade cerebral gliomas. *AJNR Am J Neuroradiol* 2002; 23: 520–527.
8. Lee HY, Na DG, Song IC, et al. Diffusion-tensor imaging for glioma grading at 3-T magnetic resonance imaging: analysis of fractional anisotropy and mean diffusivity. *J Comput Assist Tomogr* 2008; 32: 298–303.
9. Stadlbauer A, Ganslandt O, Buslei R, et al. Gliomas: histopathologic evaluation of changes in directionality and magnitude of water diffusion at diffusion-tensor MR imaging. *Radiology* 2006; 240: 803–810.
10. Jensen JH, Helpern JA, Ramani A, et al. Diffusional kurtosis imaging: the quantification of non-gaussian water diffusion by means of magnetic resonance imaging. *Magn Reson Med* 2005; 53: 1432–1440.
11. Wu EX and Cheung MM. MR diffusion kurtosis imaging for neural tissue characterization. *NMR Biomed* 2010; 23: 836–848.
12. Hui ES, Cheung MM, Qi L, et al. Towards better MR characterization of neural tissues using directional diffusion kurtosis analysis. *Neuroimage* 2008; 42: 122–134.
13. Raab P, Hattingen E, Franz K, et al. Cerebral gliomas: diffusional kurtosis

imaging analysis of microstructural differences. *Radiology* 2010; 254: 876–881.
14. Van Cauter S, Veraart J, Sijbers J, et al. Gliomas: diffusion kurtosis MR imaging in grading. *Radiology* 2012; 263: 492–501.
15. Bai Y, Lin Y, Tian J, et al. Grading of Gliomas by using Monoexponential, Biexponential, and stretched exponential diffusion-weighted MR imaging and diffusion Kurtosis MR imaging. *Radiology* 2016; 278: 496–504.
16. Reese TG, Heid O, Weisskoff RM, et al. Reduction of eddy-current-induced distortion in diffusion MRI using a twice-refocused spin echo. *Magn Reson Med* 2003; 49: 177–182.
17. Falangola MF, Jensen JH, Babb JS, et al. Age-related non-Gaussian diffusion patterns in the prefrontal brain. *J Magn Reson Imaging* 2008; 28: 1345–1350.
18. Veraart J, Poot DH, Van Hecke W, et al. More accurate estimation of diffusion tensor parameters using diffusion Kurtosis imaging. *Magn Reson Med* 2011; 65: 138–145.
19. Veraart J, Van Hecke W and Sijbers J. Constrained maximum likelihood estimation of the diffusion kurtosis tensor using a Rician noise model. *Magn Reson Med* 2011; 66: 678–686.
20. Van Cauter S, De Keyzer F, Sima DM, et al. Integrating diffusion kurtosis imaging, dynamic susceptibility-weighted contrast-enhanced MRI, and short echo time chemical shift imaging for grading gliomas. *Neuro Oncol* 2014; 16: 1010–1021.
21. Garcia-Perez AI, Lopez-Beltran EA, Kluner P, et al. Molecular crowding and viscosity as determinants of translational diffusion of metabolites in subcellular organelles. *Arch Biochem Biophys* 1999; 362: 329–338.
22. Gibbs P, Liney GP, Pickles MD, et al. Correlation of ADC and T2 measurements with cell density in prostate cancer at 3.0 Tesla. *Invest Radiol* 2009; 44: 572–576.
23. Gauvain KM, McKinstry RC, Mukherjee P, et al. Evaluating pediatric brain tumor cellularity with diffusion-tensor imaging. *AJR Am J Roentgenol* 2001; 177: 449–454.
24. Maier SE, Sun Y and Mulkern RV. Diffusion imaging of brain tumors. *NMR Biomed* 2010; 23: 849–864.